Risk-based fatigue assessment of orthotropic steel decks

Heng, Junlin; Dong, You; Baniotopoulos, Charalampos; Kaewunruen, Sakdirat

DOI:
10.1201/9781003323020

Document Version
Publisher's PDF, also known as Version of record

Citation for published version (Harvard):
Heng, J, Dong, Y, Baniotopoulos, C & Kaewunruen, S 2023, Risk-based fatigue assessment of orthotropic steel decks. in F Biondini & DM Frangopol (eds), *Life-cycle of structures and infrastructure systems: Proceedings of the eighth international symposium on life-cycle civil engineering (IALCCE 2023), 2-6 July, 2023, Politecnico Di Milano, Milan, Italy.* 1 edn, Life-Cycle of Civil Engineering Systems, Taylor & Francis, London, pp. 1975-1982, Eighth International Symposium on Life-Cycle Civil Engineering, Milan, Italy, 2/07/23.
https://doi.org/10.1201/9781003323020

Life-Cycle of Structures and Infrastructure Systems – Biondini & Frangopol (Eds)

Risk-based fatigue assessment of orthotropic steel decks

J. Heng
Shenzhen University, Shenzhen, China
University of Birmingham, Birmingham, UK

Y. Dong
The Hong Kong Polytechnic University, Hong Kong, China

C. Baniotopoulos & S. Kaewunruen
University of Birmingham, Birmingham, UK

ABSTRACT: The orthotropic steel deck (OSD) shows notable superiorities in bridge applications but is highly prone to fatigue cracking due to the use of massive welded connections, especially in the rib-to-deck (RD) connection. This study presents a risk-based approach to planning different management strategies for OSDs under fatigue, which is supported by the integrated fatigue assessment coupling test data, in-situ measurements and probabilistic simulations. RD connections are focused on since they account for the longest welding length, i.e., about 50 times the total bridge length. The probability-stress-life (P-S-N) curve is first derived for RD connections from fatigue test data. Meanwhile, a condition-based probabilistic model of vehicle loads is constructed using the site-measured data. The load model is then implemented with numerical simulations in a sampling-based manner to derive fatigue stress spectra of different fatigue-critical RD connections. Based on the derived P-S-N curve and stress spectra, the fatigue deterioration of RD connections is assessed in a probabilistic form. Moreover, the failure assessment diagram (FAD) is derived for OSDs considering the serviceability, in accordance with the estimation of associated consequences. Based on the probabilistic estimation, the risk assessment is carried out for the OSD by combining the probability of failure and associated consequences.

1 INTRODUCTION

The orthotropic steel deck (OSD) is a highly redundant and integrated deck system that is extensively employed in large-span bridges, in which the light self-weight is of the first priority (Zou et al., 2022). The OSD consists of massive components connected via a copious number of welded connections (Heng et al., 2022). Especially, the rib-to-deck (RD) welded joint can even account for 50 times the total bridge length. Under this situation, fatigue cracking is frequently observed in OSDs after several decades of exploitations (Connor et al., 2012). As a result, the normal operation of the bridge will be greatly affected in the presence of excessive cracks within the same lane.

The fatigue issue of RD joints in OSDs has already been investigated with great efforts in the past 20 years due to its prominence and notable influence, including both fatigue resistance (Cheng et al., 2016), life prediction (Ye et al. 2017), and repair methods (Wang et al., 2021). However, some further efforts are still lacking from the aspect of risk assessments, which helps to offer different insights into the recurring fatigue cracking issue of OSDs.

This work aims to offer novel insights into the fatigue-induced risk of lane closures in the OSD bridge, which can provide constructive supports for the further management of OSDs with massive welded joints. In section 2, stress spectra of RD joints in different lateral locations are derived by combing the finite element simulation and condition-based random vehicle model. In section 3, fatigue prognosis is carried out using a multi-level failure assessment diagram, followed by the associated risk assessment of lane closures. In section 4, the major result and findings are discussed. Finally, key conclusions are drawn in Section 5.

DOI: 10.1201/9781003323020-242

2 DERIVATION OF FATIGUE STRESS

2.1 *Illustration of the investigated bridge*

In this study, a typical OSD bridge in the urban network of Chengdu, China is selected as the prototype, as shown in Figure 1. The selected bridge consists of three spans of 45 m (side), 68 m (main) and 45 m (side). In the length, the bridge is divided into a total of 112 segments, each of which has a similar configuration except for the varying sectional height. The width of bridge (in a single direction) is 12.5 m, carrying one fast lane, one middle lane and one slow lane. Beneath the three lanes, a total of 15 longitudinal ribs (also called as U-ribs) are distributed. Each U-rib is connected to the deck by two RD joints on its left and right sides. For better illustration, the U-ribs are named as 1 to 15 from left (fast lane) to right (slow lane), e.g, U1. Accordingly, the associated RD joint is coded with L (left) or R (right), e.g., U1L or U1R.

Figure 1. The typical OSD bridge selected for investigation (courtesy of *Dr* Junlin HENG).

2.2 *Site-specific random traffic modelling*

Based on the site-specific traffic data, the random vehicle load (RVL) model (Heng et al., 2019) can be established to simulate the fatigue action on RD joints by vehicles, as shown in Figure 2. In the RVL model, vehicles are classified into a total of six categories, mainly depending on the configuration of axles and functions. It can be found that, the light-weight car accounts for the highest proportion in both the three lanes, i.e., 76.67% in total traffic. Meanwhile, it is worth noting that the heavy trucks V5 and V6 show a highly similar occupancy rate in the middle and slow lanes. As a result, equal concerns should be paid to the fatigue cracking in RD joints of both the middle and slow lanes.

Instead of the gross vehicle weight, the load of each vehicle type is modelled in detail from axle-to-axle. Due to the presence of multi-peaks in the distribution of axle weights, the Gaussian mixed model (GMM) model is leveraged. Meanwhile, the lateral distribution of vehicle within the lane is also considered by fitting the discrete distribution by Eurocode 1 (CEN, 2003) to a Gaussian distribution. Further details about the RVL model could be found in (Guo et al., 2015).

Based on the RVL model, random sampling of vehicles can be carried out in a conditional sampling manner, as illustrated by Equation 1,

$$p(W_i) = p(VC) \cdot p(W_i|VC) \tag{1}$$

where VC standards for the vehicle category; W_i is the weight of the ith axle.

Meanwhile, in terms of the average daily traffic (ADT), the mean value of 10,605 and standard deviation of 2,121 can be derived from the observation data.

Category	Illustration	Occupancy rate (%)		
		Fast	Middle	Slow
V1		41.23	25.74	9.70
V2		0.03	0.26	0.36
V3		0.1	0.87	0.6
V4		0.04	0.67	0.92
V5		0.06	1.17	1.31
V6		0.57	7.94	8.43

Figure 2. Configuration of different vehicle types and lane occupancy rate.

2.3 *FE-based derivation of fatigue stress*

Multi-scale finite element (FE) model of the bridge is constructed, as shown in Figure 3. The model includes the global model of the bridge structure, the sub-model of the interested segment, and the local refined model of the RD joint. The 3-dimensional shell element SHELL63 is employed in the FE modelling. Since the global modelling aims to simulate the boundary condition at the structural level, a relatively coarse meshing size is employed (i.e., 50 mm in width and 100 mm in length). Then, the segment at the mid-span is selected for the sub-model, which employs a fine mesh size of 20 × 20 mm at the outer edge. Further, the RD joint is highly refined with a very fine element size of 4 mm.

The global model and sub-model are connected using the interpolation of nodal displacement at the interface, which is realised by multi-point constriction (MPC). Meanwhile, the local refine model is embedded in the sub-model by sharing nodes directly.

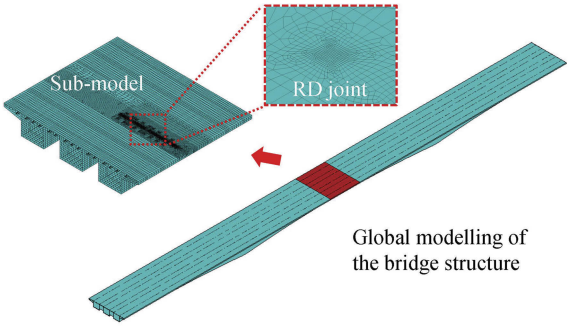

Figure 3. Finite element model of the selected bridge.

Based on the constructed FE model, the sampled vehicle can be transformed into the stress spectra of RD joints in different lateral positions, as shown in Figure 4. In the derivation, a total of 5,000,000 samples of vehicles are generated based on the RVL model discussed in Section 2.2. The influence surface technology (Heng et al., 2019) is employed to improve the solution efficiency, via which the loading of vehicles can be achieved by vector calculus. As indicated by the result, the RD joints in the fast lane (e.g., U4r) shows a low level of stress spectra due to the rare presence of heavy trucks in the lane. On the contrary, the similar RD joint in the middle lane (i.e.,

U9R) suggest a high-level stress distribution. Moreover, a very notable feature of multi-peaks can be found in the stress spectra. Moreover, the stress spectra also vary significantly within the same lane due to the lateral distribution of the car footprint. For instance, the RD joint U14L shows a very limited stress level since it is very close to the centre of the lane.

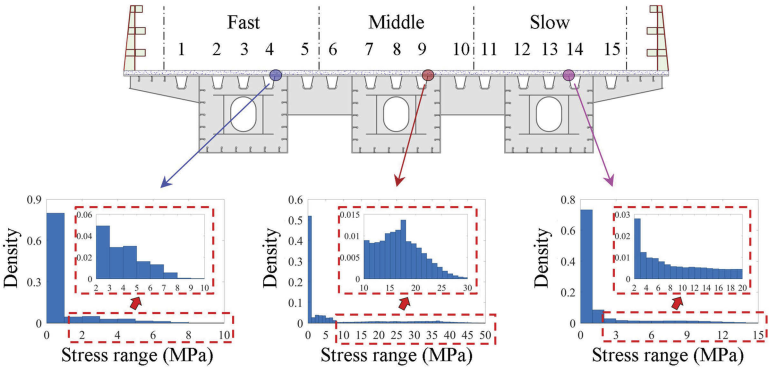

Figure 4. Stress spectra of different RD joints.

3 PROBABILISTIC PROGNOSIS AND RISK ASSEMENT

3.1 *Fatigue damage model*

The fatigue strength of RD joint is described using the probability-stress-life (P-S-N) curve, as illustrated by Equation 2,

$$\log(C) = m \cdot \log\left(\Delta\sigma_{ref}\right) + \log\left(N_{ref}\right) + \varepsilon \tag{2}$$

where C is a material constant marking the fatigue strength of RD joints; m is the power index, fixed as 3.0 in this work; $\Delta\sigma_i$ and N_i are respectively reference stress range and associated allowance number of loading cycle; ε stands for the uncertainty factor, which follows the lognormal distribution.

Based on the fatigue test data in (Zheng et al., 2019), the mean value of parameter C is determined as 2.27×10^{12}, while its coefficient of variance (COV) is solved as 0.59. For each RD joint, the fatigue limit state function (LSF) can be expressed by Equation 3,

$$g(D,t) = \Delta - D(t) \tag{3}$$

where $D(t)$ is the damage accumulation factor at time t; Δ is the tolerance factor, assumed as 1.0 in this study.

Since the RD joint experience variant-amplitude fatigue action, the linear damage accumulation rule is employed in calculating the fatigue damage, as illustrated by Equation 4,

$$D(t) = \sum_i \frac{N_i \cdot {\Delta\sigma_i}^m}{N_{ref} \cdot {\Delta\sigma_{ref}}^m} \tag{4}$$

where $\Delta\sigma_i$ and N_i denote the ith applied stress range and number of loading cycle, respectively.

3.2 *Failure assessment diagram and limit state functions*

As aforementioned, the bridge is divided into 112 segments in the length direction. Accordingly, each lane can be also divided into 112 lane segments (LSs). Moreover, as depicted in Figure 4, each lane segment has five U-ribs and ten RD joints associated. To this end, the OSD system is idealized into a link-parallel mixed system, as indicated by the failure

assessment diagram (FAD) in Figure 5. In general, the OSD system consists of three parallel components, i.e., fast, middle and slow lanes. Then, each lane is further discretized into 112 LSs, which are also in the parallel relation. Finally, each LS is modelled by a linking system covering all the ten RD joints with the lane.

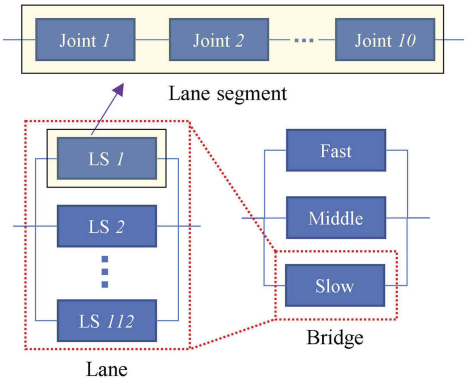

Figure 5. Failure assessment diagram of the OSD bridge.

As discussed earlier, excessive fatigue cracking within the same lane will result in mandatory lane closure due to its influence on the running safety of vehicles. To this end, after consulted with industrial colleague, the failure of the lane is assumed when the fatigue crack occurs in more than 10% of the 112 LSs, i.e., above 11 LSs. To this end, the possibility of occurrence can be further expressed for the closure in each lane, as illustrated by Equation 5,

$$p_{lc} = p\left(N_{f,LS} \geq 11\right) \tag{5a}$$

$$p_{f,LS} = \prod_{i=1}^{10} p_{f,joint}(i) \tag{5b}$$

where P_{ic} denotes the possibility of lane closure; $N_{f,LS}$ is the number of cracked lane segment; $P_{f,LS}$ is the failure probability of each lane segment; $P_{f,joint}$ (i) stands for the failure probability of ith RD joint in the lane.

3.3 *Risk assessment model*

Based on the above FAD, three scenarios are identified for potential risk of lane closures, i.e., one lane closure, two lanes closure and all the three lanes closure (i.e., the shutdown of the bridge). Accordingly, the associated costs can be estimated, as illustrated by Equation 6,

$$C_{LC} = \left(C_r + C_f + C_t\right) \cdot (1 + r_m)^t \tag{6}$$

where C_{LC} is the total cost for lane closure; C_r denotes the estimated repair cost; C_f is the fuel and abrasion cost of vehicles due to detour; Ct stands for the time value consumed by detour of vehciles; r_m is the annual discount rate of money, assumed as 1.5% in this study.

Detailed computation of the cost can be referred to a previous study (Zhu et al., 2016), while Table 1 lists the value considered in this study.

4 RESULT AND DISCUSSION

4.1 *Fatigue reliability*

Based on the proposed method, the fatigue reliability of each joint can be at first predicted, as shown in Figures 6a and b. Overall, the RD joints in the fast lane demonstrate the highest

Table 1. Key parameters for the consequence analysis.

Type	Symbol	Scenario of lane closure (in €)		
		One lane	Two lanes	Shutdown
Repair cost	C_r	93,000	166,183	230,247
Fuel cost	C_f	107,376	214,751	322,127
Time value	C_t	158,459	316,918	475,378

reliability due to the rare presence of heavy trucks. Meanwhile, very similar reliability can be found in the RD joints within the middle and slow lane, which is consistent with the distribution of heavy trucks V5 and V6. Figure 6b further plot a list of representative RD joints in the different lane. It is worth noting that the fatigue reliability of the RD joint is highly sensitive to its lateral position in the lane. For instance, the joint U14L shows the highest reliability while the nearby U14R suggests the third lowest reliability. Meanwhile, it is also revealed that the joint U12L in the slow lane is the most fatigue-critical detail. Based on the reliability prediction made using site-specific data, a tailored managing plan can be stipulated for the OSD bridge.

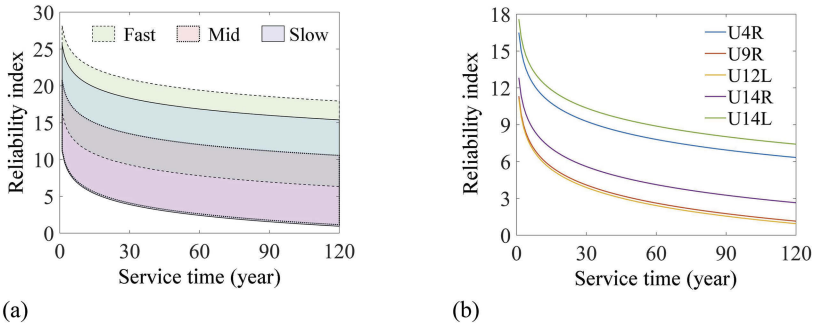

Figure 6. Reliability of welded joints: (a) distribution over lanes; (b) selected joints in different lanes.

Similarly, incorporating the FAD proposed in Figure 5, the fatigue reliability can be also assessed at the level of lane segments, as shown in Figure 7. Similar to the previous result, the middle and slow lanes show a very consistent evolution of reliability during the service life of the bridge. Meanwhile, a very prominent reliability is predicted for the fast lane due to the rare passing of heavy trucks.

In addition, the possibility of occurrence can also be estimated for the closure in different lanes, as shown in Figure 8a. Also, the fast lane is highly unlike to closure due to the limited fatigue damage by light-weight cars. At the same time, the possibility of closure becomes very prominent in both the slow lane and middle lane as the bridge is approaching the end of its design life (i.e., 120 years in this study). Moreover, the three assumed scenarios are also investigated, as shown in Figure 8b. After about 80 years of service, the closure of a single lane becomes very notable. With the time further increase, the closure of two lanes is even apparent, while the closure of a single lane becomes unlikely. At the same time, the shutdown (i.e., the closure of all the three lane) seems to be a rare event during the entire service life.

4.2 *Time-variant risk*

The time-variant risk associated with the above different scenarios is also estimated, as shown in Figures 9a and b. Overall, the risk is relatively moderated before 80 years, indicating the guaranteed performance of OSDs as a highly integrated and redundant deck system. Meanwhile, it can be found that the largest risk originates from the scenario that two lanes are forced to closure. Figure 9b further investigates the contribution of the three scenarios.

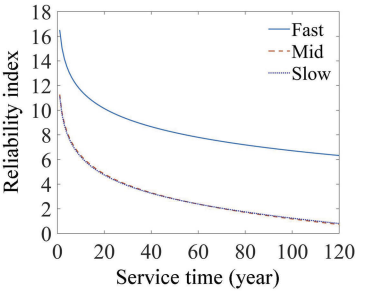

Figure 7. Reliability of lane segment.

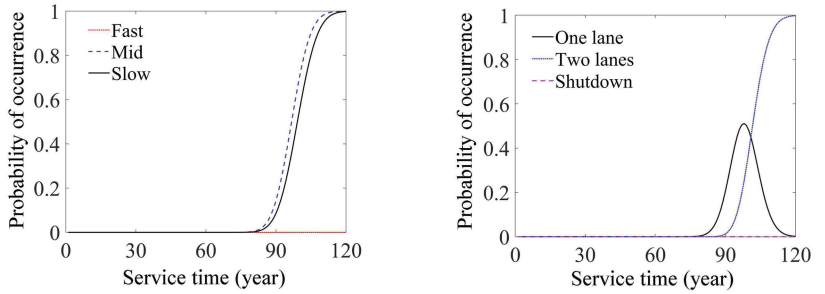

Figure 8. Probability of occurrence of lane closures: (a) different lane; (b) different scenarios.

Obviously, the "two lanes" event increase at a rapid rate and surpass the "one lane" event after roughly 100 years.

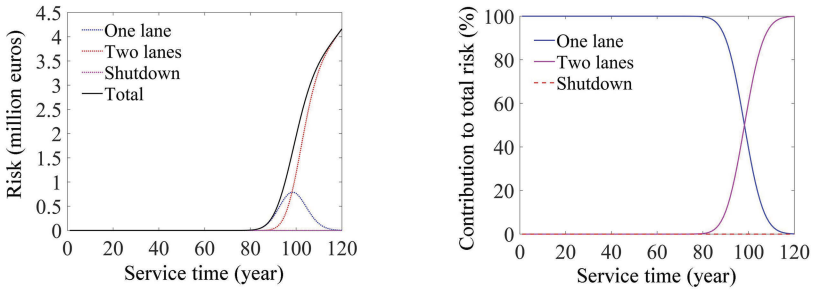

Figure 9. Time-variant risk due to fatigue: (a) different scenarios; (b) contribution of scenarios.

5 CONCLUSIONS

Based on the above investigation, the following key conclusions can be drawn.

(1) The fatigue stress spectra in the rib-to-deck (RD) joints of orthotropic steel deck (OSD) bridges are controlled by both the lane type and lateral position within the lane. Due to the rare presence of heavy trucks in the fast lane, the stress level in all the RD joints is relatively low within the lane. Meanwhile, high fatigue stress is likely to occur in the RD joint close to the frequent foot print of vehicles. Accordingly, the fatigue damage of RD joints shows a very high sensitivity to the lane type lateral position within in the lane.

(2) Both the middle lane and slow lane shows a similar possibility of closure, while it is a rare event for the closure of the fast lane. Different from the middle lane and slow lane, heavy trucks rarely select the fast lane. As a result, the mandatory closure of the slow lane is very unlikely to occur under the investigated traffic. To this end, more efforts are suggested to the slow lane and middle lane.
(3) The one-lane and two lanes closure contribute remarkably to the risk of lane closure, while the shutdown scenario has little contribution. After about 80 years of service, the risk associated with the closure of a single lane becomes very notable, which is then surpassed by the closure of two lanes soon. Meanwhile, the risk of a shutdown is maintained at a very limited level during the entire service life.

ACKNOWLEDGEMENT

The support by National Natural Science Foundation of China (52208182), Natural Science Foundation of Shenzhen (JCYJ20220531101010020) and Marie Sklodowska-Curie Actions (MSCA) Fellowship via URKI (EP/X022765/1) is acknowledged with thanks by the authors.

REFERENCES

Connor, R. J. (2012). Manual for design, construction, and maintenance of orthotropic steel deck bridges (No. FHWA-IF-12-027). United States. Federal Highway Administration.

Cheng, B., Ye, X., Cao, X., Mbako, D., & Cao, Y. (2017). Experimental study on fatigue failure of rib-to-deck welded connections in orthotropic steel bridge decks. International Journal of Fatigue, 103, 157–167.

CEN (European committee for standardization), EN 1991-2:2003 Eurocode 1: Actions on structures–part 2: traffic loads on bridges, CEN, Brussels, 2003.

Guo, T., Liu, Z., Pan, S., & Pan, Z. (2015). Cracking of longitudinal diaphragms in long-span cable-stayed bridges. Journal of Bridge Engineering, 20(11), 04015011.

Heng, J., Zheng, K., Kaewunruen, S., Zhu, J., & Baniotopoulos, C. (2019). Dynamic Bayesian network-based system-level evaluation on fatigue reliability of orthotropic steel decks. Engineering Failure Analysis, 105, 1212–1228.

Heng, J., Zhou, Z., Zou, Y., & Kaewunruen, S. (2022). GPR-assisted evaluation of probabilistic fatigue crack growth in rib-to-deck joints in orthotropic steel decks considering mixed failure models. Engineering Structures, 252, 113688.

Wang, Y., Shao, X., Chen, J., Cao, J., & Deng, S. (2021). UHPC-based strengthening technique for orthotropic steel decks with significant fatigue cracking issues. Journal of Constructional Steel Research, 176, 106393.

Ye, X. W., Liu, T., & Ni, Y. Q. (2017). Probabilistic corrosion fatigue life assessment of a suspension bridge instrumented with long-term structural health monitoring system. Advances in Structural Engineering, 20(5),674–681.

Zheng, K., Feng, X., Heng, J., Zhu, J., & Zhang, Y. (2019). Fatigue reliability analysis of rib-to-deck joints using test data and in-situ measurements. Applied Sciences, 9(22), 4820.

Zhu, B., & Frangopol, D. M. (2016). Time-variant risk assessment of bridges with partially and fully closed lanes due to traffic loading and scour. Journal of Bridge Engineering, 21(6), 04016021.

Zou, Y., Yu, K., Heng, J., Zhang, Z., Peng, H., Wu, C., & Wang, X. (2022). Feasibility study of new GFRP grid web-concrete composite beam. Composite Structures, 116527.